DOI: https://doi.org/1015407/techned2021.03.058

SIMULATION OF MOBILE ROBOT CLAMPING MAGNETS BY CIRCLE-FIELD METHOD

O.O. Cherno*, O.S. Gerasin, A.M. Topalov, D.K. Stakanov, A.P. Hurov, Yu.O. Vyzhol**
Admiral Makarov National University of Shipbuilding,
9, Heroev Ukrainy Av., Mykolaiv, 54025, Ukraine. **E-mail:** **alextcherno@gmail.com**

There are a list of complicated tasks need to be solved to increase the working productivity and decrease working cost in modern shipbuilding and ship repair. Good results in solving those problems are shown whether automation with varied robots implementation. The mobile robots able to move and perform given technological operations on different-spaced ferromagnetic surfaces are equipped with own control systems, movers and clamping devices. Usually, reliability and safety of such robots are in direct dependence on designers' adequate representation of their behavior that is described by mathematical description of separate parts or the robot in the whole to correct control problem solving. The article amply considers the process of the climbing mobile robot clamping electromagnet simulation model building using the improved circle-field method on the example of BR-65/30 clamping electromagnet. The model is built on the basis of interpolated dependences of flux coupling and electromagnetic force on the magnetomotive force and the value of the air gap obtained by numerical calculations of the magnetic field. The dynamic properties of the electromagnet are investigated and a family of its traction characteristics is obtained by the developed model, which can be used for automatic control of the robot clamping device. References 25, figures 5, tables 3.
Key words: clamping electromagnets, mobile robot, modeling, circle-field method, traction characteristics.

Introduction. Increasing labor productivity and reducing the cost of finished products or services in modern conditions is achieved by increasing the level of automation of production, including by using robotic systems and complexes that replace humans when performing time-consuming and dangerous to human life and health technological operations [1-3]. Particularly important role is played by flexible mobile robots, which are able to move the work tool on both flat and complex sloping surfaces [4, 5]. In particular, in shipbuilding and ship repair the use of mobile robots on ferromagnetic surfaces of ship hulls is promising for automation of multi-purpose technological operations and tasks: cleaning of large areas, painting, cutting, welding, inspection, diagnostics, rescue operations and fire safety, operating in aggressive and high-temperature environments, hard-to-reach places, etc. [4-8].

Mobile robotic complexes are equipped with clamping permanent magnets or controlled electromagnets to ensure reliable retention and movement on the ferromagnetic surface [9]. The electromagnet as an element of the automatic control system of clamping force has better controllability than pneumatic and hydraulic clamping devices of mobile robots [10-11]. When designing robots with a fixed gap between the clamping magnet and the working ferromagnetic surface, there is a problem of choosing the optimal number of clamping magnets with a certain value of the nominal clamping force for reliable movement and adhesion to the surface without slipping [12, 13]. Therefore, the development and improvement of models and methods, that will take into account the electromagnetic and electromechanical processes of interaction of the clamping electromagnet and the ferromagnetic surface, is an urgent task to improve the efficiency and reliability of advanced control systems of such mobile robots with working surfaces [3, 12, 14, 15].

Analysis of previous research. For joint simulation of electromagnetic, electromechanical and mechanical processes, it is advisable to use the circle-field method [16]. When applied to electromagnets it allows to determine the instantaneous values of electromagnetic force and flux coupling depending on the value of the air gap and the voltage supplied to the winding [17]. The essence of the method is a numerical calculation of the spatial magnetic field taking into account the nonlinearity of the magnetic circuit magnetization characteristics for a fixed position of the electromagnet armature and a fixed value of direct current in the winding [18, 19]. Next, the amount of magnetic flux linkage is determined integrating the magnetic induction by the area of the winding turns:

$$\psi = \sum_{j=1}^{W} \int_{S_{wj}} \mathbf{Bn}_{wj} dS_{wj} ,$$

ORCID ID: * https://orcid.org/0000-0003-1670-8276; ** https://orcid.org/0000-0003-2745-7388

where S_{wj} is the area of the j-th turn of the winding; **B** is the vector of magnetic induction; $\mathbf{n}_{wj}$ is the normal to the plane of the *j*-th turn of the winding. The vector of electromagnetic force $\mathbf{F}_e$ acting on the armature of the electromagnet is determined according to Maxwell's formula [20]:

$$\mathbf{F}_e = \frac{1}{\mu_0}\oint_S \left((\mathbf{Bn})\mathbf{B} - \frac{1}{2}B^2\mathbf{n} \right) dS ,$$

where *S* is the surface of the anchor; **n** is the normal vector to the anchor surface. If the vector $\mathbf{F}_e$ is directed along the tracking direction of the armature then $F_e = |\mathbf{F}_e|$.

Similarly, the values of flux linkage and electromagnetic force are determined for a number of combinations of the air gap values and direct current in the winding. The results of the calculations are entered in two tables showing the dependences of the flux linkage ψ and the electromagnetic force F_e on the value of the air gap δ and the magnetomotive force of the winding *IW*. As a result of tabular dependences approximation, continuous functions $\psi(IW,\delta)$ and $F_e(IW,\delta)$ are obtained, which are then used in solving the equations of the electromagnet winding electric circuit combined with the equations of mechanics.

In the articles [21, 22] an improved circle-field method is used. It includes the transformation of the direct dependences ψ(*IW*) to inverse dependences *IW*(ψ) for a number of δ values. This eliminates the need for flux linkage differentiation in the numerical equation solution, and thus increases the accuracy of the simulation. Therefore, this modification of the method is most suitable for modelling clamping electromagnets of mobile robots.

The aim of this research was to develop a simulation model of electromagnetic and electromechanical processes in the clamping electromagnets of mobile robots using the circle-field method.

Designing a model of the mobile robot clamping magnet in Ansoft Maxwell. It is advisable to use clamping electromagnets BR-65/30 (Fig. 1, *a*) in the considered mobile robots. The main characteristics of the electromagnet [23] are: rated voltage 12 V; rated current 1.08 A; rated power 13 W; rated clamping force 800 N; winding inductance 75 mH (according to the measurement results).

A specialized program Ansoft Maxwell was used for numerical calculations of electromagnetic force and magnetic flux linkage of electromagnets when varying the values of the magnetomotive force and air gap [19, 24]. The three-dimensional model of the electromagnet is built in the graphic editor of the Ansoft Maxwell and presented in Fig. 1, *b*, where *1* − electromagnet core; *2* − winding; *3* − ferromagnetic disk to which the electromagnet is attracted. The diameter of the disk is chosen to be twice the diameter of the electromagnet to eliminate the influence of the edge effect. Then a number of magnetomotive force values are programmatically set. Two tables of magnetic flux linkage values (Table 1) and electromagnetic force values (Table 2) are obtained as a result of computer simulation.

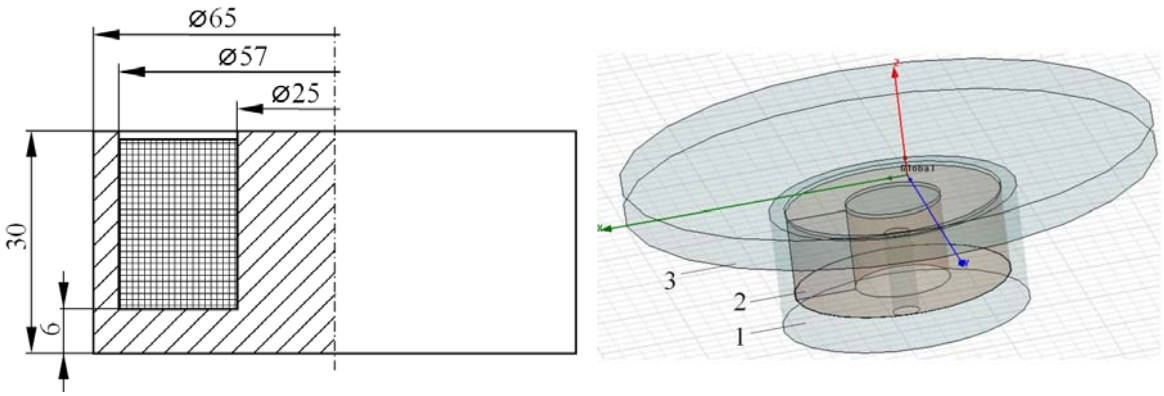

a ***b***

Fig. 1

Since in the future the magnetic flux linkage function will be approximated by the least squares method, and the electromagnetic force function will be interpolated by cubic splines, it requires a larger number of calculation points (Table 2).

Table 1

δ, mm	*IW*, kA											
	0.1	0.25	0.5	1	1.5	2	3	4	6	8	10	12
	ψ, mWb											
0.05	0.430	0.730	0.837	0.885	0.925	0.955	1.013	1.068	1.174	1.277	1.376	1.468
0.1	0.298	0.647	0.812	0.875	0.915	0.948	1.007	1.063	1.170	1.272	1.372	1.465
0.175	0.204	0.498	0.762	0.863	0.902	0.941	0.996	1.054	1.163	1.265	1.364	1.458
0.25	0.158	0.393	0.697	0.853	0.891	0.929	0.987	1.045	1.155	1.259	1.358	1.453
0.35	0.125	0.312	0.597	0.834	0.877	0.916	0.979	1.035	1.144	1.251	1.350	1.445
0.5	0.096	0.241	0.475	0.786	0.859	0.895	0.965	1.016	1.131	1.237	1.339	1.435
0.75	0.072	0.181	0.360	0.681	0.827	0.868	0.938	1.002	1.107	1.217	1.319	1.416
1	0.059	0.147	0.294	0.577	0.776	0.842	0.910	0.981	1.088	1.196	1.298	1.399
1.5	0.045	0.113	0.226	0.449	0.657	0.789	0.874	0.936	1.060	1.159	1.263	1.362
2	0.038	0.094	0.188	0.375	0.559	0.715	0.841	0.904	1.022	1.132	1.229	1.328
3	0.029	0.073	0.147	0.295	0.440	0.581	0.780	0.851	0.968	1.070	1.181	1.271
4	0.025	0.063	0.126	0.253	0.379	0.503	0.719	0.813	0.925	1.033	1.136	1.235
5	0.023	0.057	0.114	0.227	0.342	0.454	0.663	0.778	0.898	1.002	1.089	1.199

Table 2

δ, mm	*IW*, kA															
	0.1	0.25	0.35	0.5	0.75	1	1.25	1.5	2	2.5	3	4	6	8	10	12
	F_e, N															
0.05	212	613	717	801	860	899	938	977	1030	1077	1123	1210	1382	1551	1707	1828
0.1	94.1	489	590	701	783	823	859	894	953	1000	1042	1127	1290	1453	1603	1736
0.175	41.1	243	412	570	692	735	770	803	866	913	955	1036	1191	1345	1487	1626
0.25	23	141	266	445	599	663	697	730	790	842	883	961	1110	1256	1397	1526
0.35	12.9	80.5	156	300	490	584	621	651	708	762	807	882	1025	1164	1298	1426
0.5	6.94	43.3	84.4	170	343	465	529	560	614	664	712	787	923	1056	1183	1307
0.75	3.37	21.1	41.3	83.9	185	303	393	448	500	546	590	668	796	920	1041	1158
1	2.01	12.6	24.6	50.2	112	194	281	349	418	460	499	575	698	814	930	1042
1.5	0.97	6.06	11.9	24.3	54.5	96.3	148	205	299	343	376	441	557	659	761	865
2	0.578	3.61	7.08	14.4	32.5	57.5	89.6	127	208	265	297	351	455	548	638	730
3	0.277	1.73	3.39	6.92	15.5	27.6	43.1	61.9	108	158	195	239	318	395	468	541
4	0.162	1.01	1.99	4.05	9.13	16.2	25.3	36.4	64.2	97.7	131	171	234	295	355	414
5	0.106	0.663	1.3	2.65	5.96	10.6	16.6	23.8	42.2	65	90.1	127	177	226	275	323

Approximation of the magnetic field calculation results. The dependences $\psi_j(IW)$ can be approximated by hyperbolic functions [25]:

$$y_j(x) = \left(y_{c_j} - k_{r_j} x_{c_j}\right)\left(1 - \left[\left(x - x_{c_j}\right)^2 + {b_j}^2\right]^{1/2}\left[x_{c_j}^2 + b_j^2\right]^{-1/2}\right) + k_{r_j} x,$$

where j is the row number of Table 1; (x_c, y_c) are the coordinates of the center of the hyperbola; b is the value that sets the focal length; k_r is the coefficient of rotation.

All 4 coefficients of the approximating function are determined by the method of least squares by searching in 4 nested loops for one of the dependences (j = 6, δ = 0.5 mm), so the slope of the upper asymptote, which is the same for all hyperbolas $y_j(x)$, is found as:

$$k_a = \left(k_{r_6} x_{c_6} - y_{c_6}\right)\left(x_{c_6}^2 + b_6^2\right)^{-1/2} + k_{r_6} = 5.198 \text{ Wb/A}.$$

When approximating other dependencies a search of values x_c, y_c and b is performed in 3 nested loops determining the value of k_r by the formula:

$$k_r = \left(y_c\left(x_c^2 + b^2\right)^{-1/2} + k_a\right)\left(x_c\left(x_c^2 + b^2\right)^{-1/2} + 1\right)^{-1}.$$

The resulting vectors of the hyperbola coefficients:

$$\mathbf{x_c} = (133 \quad 232 \quad 354 \quad 482 \quad 621 \quad 810 \quad 1103 \quad 1348 \quad 1762 \quad 2100 \quad 2644 \quad 3012 \quad 3278)^T \text{ (A)};$$

$$\mathbf{y_c} = (0.867 \quad 0.866 \quad 0.866 \quad 0.864 \quad 0.864 \quad 0.862 \quad 0.856 \quad 0.85 \quad 0.836 \quad 0.822 \quad 0.796 \quad 0.774 \quad 0.752)^T \text{ (mWb)};$$

$$\mathbf{b} = (121 \quad 150 \quad 198 \quad 222 \quad 262 \quad 324 \quad 373 \quad 434 \quad 480 \quad 518 \quad 530 \quad 516 \quad 462)^T \text{ (A)};$$

$$\mathbf{k_r} = (2.802 \quad 1.732 \quad 1.168 \quad 0.88 \quad 0.694 \quad 0.539 \quad 0.404 \quad 0.334 \quad 0.259 \quad 0.219 \quad 0.175 \quad 0.154 \quad 0.14)^T \text{ (mWb/kA)}.$$

The graphs of the dependencies $\psi_j(IW)$ are shown in Fig. 2.

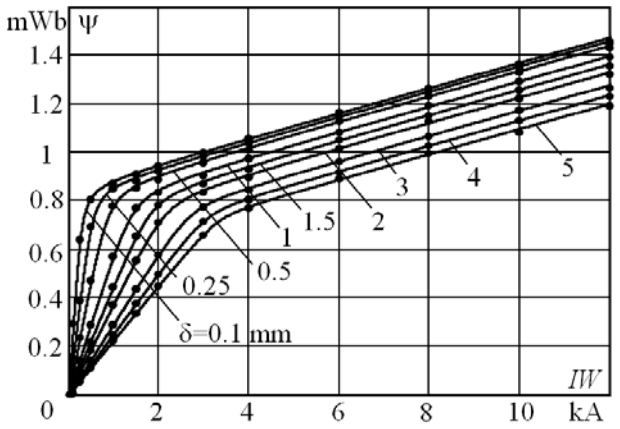

Fig. 2

Then we set a range of flux linkage values:

$$\Psi_k = k\Delta\psi ,$$

where k = 0, 1, ... 15; $\Delta\psi$ = 0.1 mWb. For each value we make the equation:

$$\psi_j(IW) = \Psi_k .$$

A number of magnetomotive force values $IW_{j,k}$, corresponding to the specified values of flux linkage Ψ_k at air gap values δ_j, is determined numerically solving these equations by the method of half division. The results are summarized in Table 3. By interpolating the table dependence we obtain the function of two variables $IW(\psi,\delta)$. This function will be used in the equations of the electric circuit of the electromagnet winding.

Table 3

δ, mm	ψ, mWb														
	0.1	0.2	0.3	0.4	0.5	0.6	0.7	0.8	0.9	1	1.1	1.2	1.3	1.4	1.5
	IW, kA														
0.1	0.032	0.065	0.099	0.136	0.176	0.224	0.293	0.453	1.24	2.95	4.83	6.73	8.65	10.6	12.5
0.25	0.062	0.124	0.188	0.254	0.325	0.404	0.506	0.706	1.54	3.24	5.11	7.01	8.93	10.8	12.8
0.5	0.101	0.204	0.308	0.415	0.527	0.651	0.802	1.07	1.96	3.64	5.5	7.39	9.3	11.2	13.1
1	0.166	0.334	0.504	0.676	0.855	1.05	1.27	1.64	2.69	4.41	6.27	8.17	10.1	11	13.9
1.5	0.218	0.437	0.658	0.883	1.11	1.36	1.64	2.09	3.29	5.06	6.94	8.84	10.8	12.7	14.6
2	0.263	0.526	0.792	1.06	1.34	1.62	1.95	2.5	3.85	5.66	7.55	9.46	11.4	13.3	15.2
3	0.338	0.677	1.02	1.36	1.71	2.07	2.49	3.22	4.8	6.67	8.57	10.5	12.4	14.3	16.3
4	0.394	0.789	1.19	1.58	1.99	2.41	2.88	3.81	5.54	7.43	9.33	11.3	13.2	15.1	17
5	0.439	0.880	1.32	1.76	2.21	2.67	3.2	4.36	6.19	8.1	10	11.9	13.9	15.8	17.7

Electromagnet equivalent circuit and process equations. Taking into account the influence of eddy currents on the nature of transients, we make an equivalent circuit of the electromagnet winding (Fig. 3). The circuit shows: R is the active resistance of the winding; values reduced to the winding: $i^*_{e.c} = i_{e.c}/W$; $R^*_{e.c} = R_{e.c}W^2$; $i_{e.c}$ is the magnetomotive force generated by eddy currents; W is the number of the winding turns; $R_{e.c}$ is the resistance to eddy currents; u, i, i_μ is the instantaneous values of winding voltage, winding current and magnetizing current, respectively.

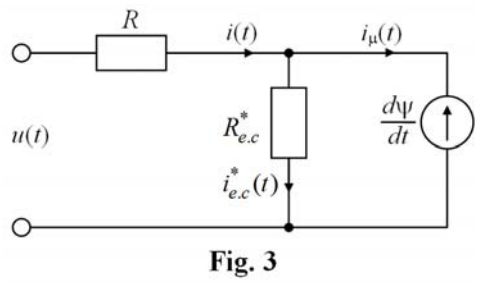

Fig. 3

Since the number of the winding turns is not given in the documentation of the electromagnet, it can be determined through the measured inductance L = 75 mH and calculated in the program Ansoft Maxwell magnetic conductivity in the open state Λ_{open} = 0,144 mkH:

$$W = \sqrt{L/\Lambda_{open}} = 722 .$$

The complex magnetic resistance has been calculated as $Z_m = R_m + jX_m = 2.2\cdot10^6 + j\cdot9.5\cdot10^3$ (H^{-1}) to determine the value of $R_{e.c}$. Wherein it was set low-frequency alternating current (ω = 1 rad/s) in the model to eliminate current displacement effect. The resistance to eddy currents is determined using the imaginary part of the complex magnetic resistance: $R_{e.c} = \omega/X_m = 10^{-4}$ Ohm.

The resistance reduced to the winding:

$$R^*_{e.c} = R_{e.c}W^2 = 52 \text{ Ohm}.$$

The equations of the electric circuit processes:

$$\frac{d\psi}{dt} = u(t) - Ri(t); \quad i(t) = i_{\mu}(t) + i^{*}_{e.c}(t); \quad i_{\mu} = \frac{1}{W} IW\left(\psi(t), \delta(t)\right); \quad i^{*}_{e.c}(t) = \frac{1}{R^{*}_{e.c}}\left(u(t) - Ri(t)\right). \qquad (1)–(4)$$

The equations (1) − (4) can be solved numerically using Rungk-Kutta method.

Development of the simulation model and calculation of electromagnet characteristics. A simulation model of the electromagnet in the Simulink environment is created based on equations (1) − (4) and Tables 1, 3 (Fig. 4). The calculation of the resulting magnetomotive force is occurred in the block "IW" by interpolating the data of Table 3 and the calculation of electromagnetic force – in the block "Magnetic force" by interpolating the data in Table 1.

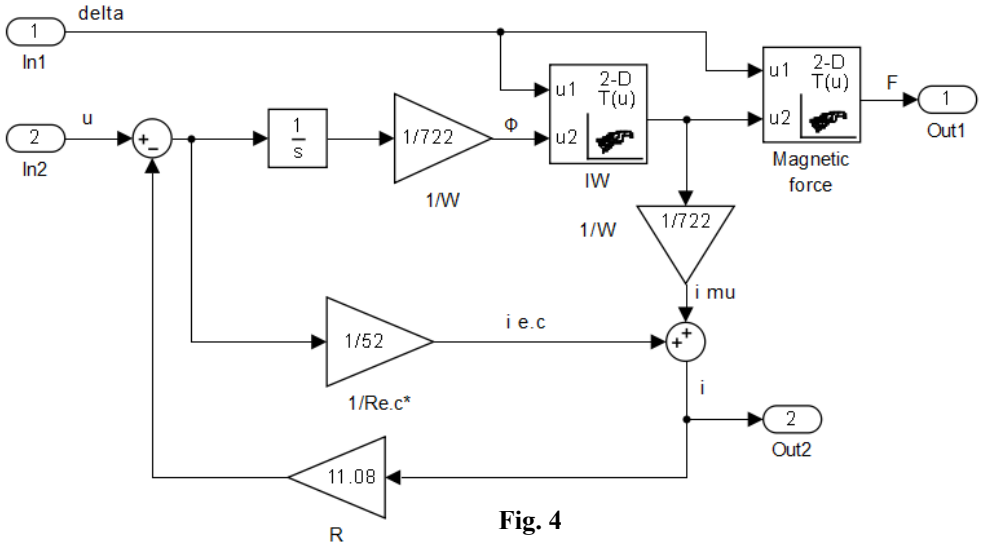

Fig. 4

The input values of the electromagnet simulation model are the instantaneous values of voltage and air gap, and the output values are the instantaneous values of the electromagnetic force and current. The electromagnet characteristics (Fig. 5) are obtained as a result of modelling.

A family of static traction characteristics is given in Fig. 5, *a*. They are the dependences of the electromagnetic force on the value of the air gap at different values of the winding current. At the rated current I_n and close to zero values of the air gap electromagnetic force is close to 800 N, which corresponds to the nominal clamping force given in the datasheet [23].

If the nominal value of the air gap between the mobile robot's clamping electromagnets and the ferromagnetic surface is 2 mm, then, according to the characteristics (Fig. 5, *a*), at rated current each electromagnet will provide a clamping force of 35 N, and double current increase will give an opportunity to briefly increase the force to 140 N to prevent detachment from the surface in case of danger. Similarly, at the beginning of the detachment (this situation can be detected by slip displacement sensors [13]), when the gap increases to 2.5 mm, a short-term increase in current to twice the nominal value will increase the force to 91 N and return the robot to the working surface.

The dynamic properties of clamping electromagnets have essential value at automatic control. Fig. 5 shows graphs of growth of electromagnetic force (Fig. 5, *b*) and winding current (Fig. 5, *c*) when the electromagnet is turned on at rated voltage for different values of the air gap. The following patterns can be observed according to the obtained graphs. As the air gap value decreases, the time of the electromagnetic force increase first increases (at the gap values less than 0.3 mm), and then decreases again. This is due to the electromagnet inductance increase by the air gap magnetic conductivity increase, and then − the inductance decrease by the steel saturation. The dynamics of the winding current change is characterized by a stepwise increase to 0.2 A due to eddy currents, and then – by a gradual increase to the nominal value. The rate of current growth also depends on the conductivity of the gap and the saturation of the magnetic circuit.

Conclusions. The use of the circle-field method for modeling clamping electromagnets of mobile robots makes it possible to create a model of electromagnetic and electromechanical processes, that takes into account the spatial distribution of the magnetic field, nonlinearity of steel magnetization characteristics and eddy currents, adding new knowledge to [12, 15, 19, 25]. The model is based on the numerically calculated dependences of flux linkage and electromagnetic force on the magnetomotive force and the value of the air gap, which were approximated and included in the equations of the electromagnet winding electric circuit. At the same time mathematical methods of approximation of dependences of flux linkage on magnetomotive force by hyperbolic functions and transition to inverse dependences were applied. The simulation model of the clamping electromagnet in the Simulink program is designed on the basis of the received equations and the calculated tabular values. The family of the traction characteristics for different winding cur-

rents, as well as the characteristics of the electromagnet at different values of the air gap are calculated. They determine the electromagnet dynamic properties as an actuator of the clamping force automatic control system. The developed simulation model of the clamping electromagnet will be used as a subsystem included as a part in the model of motion control systems for mobile robots able to move on inclined and vertical ferromagnetic surfaces.

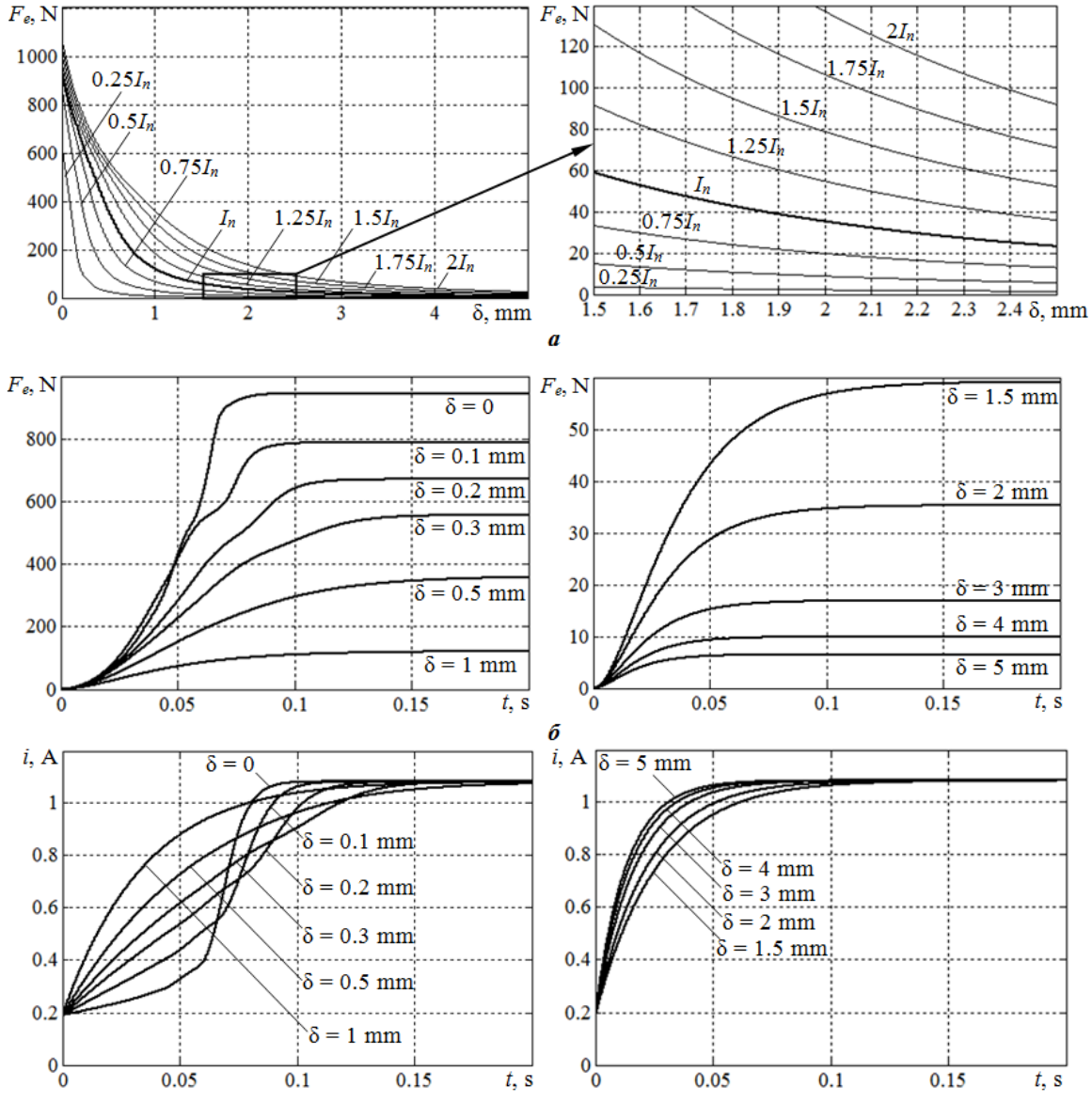

Fig. 5

1. Christensen L., Fischer N., Kroffke S., Lemburg J., Ahlers R. Cost-effective autonomous robots for ballast water tank inspection. *Journal of Ship Production and Design*. 2011. Vol. 27 (3). Pp. 127-136.

2. Ross B., Bares J., Fromme C. A semi-autonomous robot for stripping paint from large vessels. *The International Journal of Robotics Research*. 2003. Vol. 22(7-8). Pp. 617-626. DOI: https://doi.org/10.1177/02783649030227010.

3. Kondratenko Y.P., Kozlov A.V. Parametric optimization of fuzzy control systems based on hybrid particle swarm algorithms with elite strategy. *Journal of Automation and Information Sciences*. 2019. Vol. 51. Issue 12. Pp. 25-45.

4. Tosun O., Akin H.L., Tokhi M.O., Virk G.S. Mobile robotics: solutions and challenges. Proc. of the 12th International Conference on *Climbing and Walking Robots and the Support Technologies for Mobile Machines*. Istanbul, Turkey, September 9-11, 2009.

5. Taranov M., Rudolph J., Wolf C., Kondratenko Y., Gerasin O. Advanced approaches to reduce number of actors in a magnetically-operated wheel-mover of a mobile robot. Proc. of the 2017 13th International Conference *Perspective Technologies and Methods in MEMS Design (MEMSTECH)*. Polyana, Ukraine, 2017. Pp. 96-100.

6. Souto D., Faiña, A., Deibe, A., Lopez-Peña, F., Duro, R. J. A robot for the unsupervised grit-blasting of ship hulls. *International Journal of Advanced Robotic Systems*. 2012. Vol. 9. Pp. 1-16.

7. Siciliano B., Khatib O. Springer handbook of robotics. Springer, 2016. 1611 p.

8. Faina A., Orjales F., Souto D., Bellas F., Duro R. A modular architecture for developing robots for industrial applications. *Advances in Intelligent Robotics and Collaborative Automation*. River Publishers, 2015. Pp. 1-26.

9. Kondratenko Y.P., Rudolph J., Kozlov O.V., Zaporozhets Y.M., Gerasin O.S. Neuro-fuzzy observers of clamping force for magnetically operated movers of mobile robots. *Tekhnichna Electrodynamica.* 2017. No 5. Pp. 53-61. (Ukr) DOI: https://doi.org/10.15407/techned2017.05/053

10. Gradetskiy V., Rachkov M. Robots for vertical movement. Moscow: RF Ministry of Education Publisher, 1997. (Rus)

11. Souto D., Faica A., Lypez-Peca F., Duro R.J. Lappa: a new type of robot for underwater non-magnetic and complex hull cleaning. Proc. of IEEE International Conference *Robotics and Automation*. Karlsruhe, Germany, May 6-10, 2013. Pp. 3394-3399.

12. Zaporozhets Y. M., Kondratenko Y. P. Objectives and features of the control of magnetic mover wheeled mobile robot. *Elkctronnoe Modelirovanie.* 2013. Vol. 35. No 5. Pp. 109-123. (Rus).

13. Kondratenko Y., Topalov A., Gerasin O. Analysis and modeling of the slip signals' registration processes based on sensors with multicomponent sensing elements. Proc. of the 13th International Conference *CADSM 2015,* Lviv, Ukraine, February 24-27, 2015. Pp. 109-112.

14. Kondratenko Y.P., Kozlov O.V. Generation of rule bases of fuzzy systems based on modified ant colony algorithms. *Journal of Automation and Information Sciences*, 2019. Vol. 51. Issue 3. Pp. 4-25.

15. Kondratenko Y., Zaporozhets Y., Rudolph J., Gerasin O., Topalov A., Kozlov O. Modeling of clamping magnets interaction with ferromagnetic surface for wheel mobile robots. *International Journal of Computing*. 2018. No 17 (1). Pp. 33-46.

16. Vaskovskiy Yu.N. Prospects for modeling the dynamic modes of electromechanical transducers based on circle-field methods. *Electrical engineering and electromechanics*. 2003. No 1. Pp. 23-25. (Rus.)

17. Neyman L., Neyman V., Shabanov A. Vibration dynamics of an electromagnetic drive with a half-period rectifier. Proc. of 18-th International Conference of Young Specialists *Micro/nanotechnologies and Electron Devices EDM*. Novosibirsk, RF. 2017. Pp. 503-506.

18. Polivanov K.M. Theoretical foundations of electrical engineering. Part 3% Electromagnetic field theory. Moskva: Energiia, 1969. 352 p. (Rus)

19. Kondratenko Y. P., Zaporozhets Y. M., Rudolph J., Gerasin O. S., Topalov A. M., Kozlov O. V. Features of clamping electromagnets using in wheel mobile robots and modeling of their interaction with ferromagnetic plate. Proc. of the 9th IEEE International Conference *Intelligent Data Acquisition and Advanced Computing Systems: Technology and Applications (IDAACS)*. Bucharest, Romania, 2017. Vol. 1. Pp. 453-458.

20. Lvov E.L. Relationship between different methods of calculating static traction forces in electromagnetic systems. *Proceedings of the Moscow Energy Institute.* 1951. Issue VII.

21. Tcherno A.A. Dynamic model of an electromagnetic vibrating drive. *Tekhnichna Electrodynamica*. 2014. No 2. Pp. 37-43. (Rus)

22. Cherno O.O., Monchenko M.Y. Energy efficiency of the vibratory device electromagnetic drive system. *Tekhnichna Electrodynamica*. 2015. No 1. Pp. 20-25.

23. Bairun Electric Store. Electromagnet 65*30 mm, 80 kg, DC 5V/12V/24V. URL: https://goo.su/3hGb (accessed 15.11.2020)

24. Cherkasova O.A. Research of the magnetic field of the permanent magnet by means of computer modeling. URL: https://goo.su/3Hgb. (accessed 15.11.2020). (Rus)

25. Cherno O., Hurov A., Bugrim L. Peculiarities of the creating of electromagnetic vibration drive systems mathematical models. *Electromechanical and energy saving systems*. 2018. Vol. 3(43). Pp. 45-51. (Ukr)

УДК 621.318.3

МОДЕЛЮВАННЯ ПРИТИСКНИХ МАГНІТІВ МОБІЛЬНИХ РОБОТІВ КОЛО-ПОЛЬОВИМ МЕТОДОМ

О.О. Черно, канд. техн. наук, **О.С. Герасін,** канд. техн. наук, **А.М. Топалов,** канд. техн. наук, **Д.К. Стаканов, А.П. Гуров,** канд. техн. наук, **Ю.О. Вижол**, канд. фіз.-мат. наук

Національний університет кораблебудування ім. адмірала Макарова,
просп. Героїв України, 9, Миколаїв, 54025, Україна. **E-mail: alextcherno@gmail.com**

У сучасному суднобудуванні та судноремонті існує перелік складних завдань, які потрібно вирішити для підвищення продуктивності праці та зменшення основних витрат. Хороші результати у вирішенні цих завдань показує автоматизація із впровадженням різнотипних роботів. Мобільні роботи, здатні переміщуватися та виконувати задані технологічні операції на феромагнітних поверхнях різного просторового розташування, обладнують власними системами керування, рушіями та притискними пристроями. Зазвичай надійність магніта та безпека таких роботів знаходяться в прямій залежності від належного уявлення розробників щодо їхньої поведінки, яка описується математично для окремих частин або робота в цілому з метою коректного вирішення проблем керування. В статті розглянуто процес побудови імітаційних моделей притискних електромагнітів мобільних роботів з використанням покращеного коло-польового методу на прикладі електромагніта BR-65/30. Модель побудовано на основі інтерпольованих залежностей потокозчеплення та електромагнітної сили від магніторушійної сили та величини повітряного зазору, отриманих шляхом числових розрахунків магнітного поля. За допомогою розробленої моделі досліджено динамічні властивості електромагніту та отримано сімейство його тягових характеристик, що можуть бути використані для автоматичного керування притискним пристроєм. Бібл. 25, рис. 5, табл. 3.

***Ключові слова*:** затискні електромагніти, мобільний робот, моделювання, метод кругового поля, тягові характеристики.

Надійшла 06.01.2021